Preprints of the 2012 20th Mediterranean Conference on Control & Automation (MED), Barcelona, Spain, July 3-6, 2012

An Experimental Study on Thermodynamic Properties of Pneumatic Artificial Muscles

G. Andrikopoulos, G. Nikolakopoulos and S. Manesis

Abstract— **In the past fifty years, several attempts have been made to model the characteristics of Pneumatic Artificial Muscles (PAMs). PAM models based on their geometrical properties are the most commonly found ones in the scientific literature. In the process of deriving those models a lot of assumptions and simplifications are made due to the fact that PAM is a highly non-linear form of actuation. The purpose of this study is to propose additional considerations for future model improvements that will augment the overall model accuracy, and will best describe the relationship between force, displacement and non-linear thermal properties of PAM actuators through extensive observation and analysis of its thermodynamic characteristics during long-run operation experiments. In this article multiple experimental results will be presented that prove the relation between the thermodynamic properties of the PAMs, especially in iterative operations, and the accuracy on the muscle's force-prolongation relationship.**

I. Introduction

Pneumatic Artificial Muscle (PAM) [1], [2] also known as the McKibben Artificial PAM [3], [4], Pneumatic PAM Actuator or Fluidic Muscle [5], [6] is a tube–like actuator that is characterized by a decrease in the actuating length when pressurized. Best known member of this family is the McKibben–PAM, which was invented in 1950s by the physician, Joseph L. McKibben and was utilized as an orthotic appliance for polio patients [7], while the first commercialization of PAMs has been done by the Bridgestone Rubber Company of Japan in the 1980s. PAMs are significantly light actuators that are characterized by smooth, accurate and fast response and also are able to produce a significant force when fully stretched.

PAM typically consists of a long synthetic or natural rubber tube, wrapped inside man–made double helix synthetic fiber netting, made from materials like aramid, at predetermined angle. Protective rubber coating, usually made from neoprene, surrounds the fiber wrapping and appropriate metal fittings are attached at each end. The Fluidic Muscle, a PAM like the one presented in Fig.1, differs from the classic McKibben PAM as it utilizes a combined integration of the inner tube and external shell to a single aramid-neoprene mesh.

Fig. 1. Pneumatic Artificial Muscle (PAM) during contraction (top) and relaxation (bottom).

When compressed air is applied to the interior of the rubber tube, the netting causes contraction in length and radial expansion of the PAM. As the air exits, the tube acts as a spring that restores the PAM in its original form.

The PAM has many advantages over conventional pneumatic cylinders such as high force to weight ratio, variable installation possibilities, no mechanical parts, lower compressed–air consumption and low cost; as well as disadvantages such as limited fatigue life and length-variant contractile force [8]. An extensive overview of the most significant PAM applications can be found in [9].

In the past fifty years, several attempts have been made to model the characteristics of PAM. The aim of such models is to relate the pressure and length to the force it exerts along its entire axis. Variables such as pulling force, actuator's length, air pressure, diameter and material properties, play a major role on the actuator's dynamical behavior and that is why understanding the relationships between them is of paramount importance in order to best control this kind of actuator [10].

PAM models based on its geometrical properties are the most utilized ones. In the process of deriving those models a lot of assumptions and simplifications are made due to the fact that PAM is a highly non-linear form of actuation. Among its main non-linear characteristics are a) the compressibility of pressurized air, b) the viscoelastic materials, c) friction phenomena from the braid mesh threads relative motion and their contact with the inner elastic bladder and d) the complex geometric features of the outer braided shell.

In this article, an experimental study on the thermodynamic properties of PAM will be described in detail. The main novelty of this work is the extensive experimental thermal observation and analysis of PAM during long-run operation experiments. Furthermore, the relationship between the actuator's non-linear temperature

Manuscript received January 30, 2012.

G. Andrikopoulos is with the Electrical and Computer Engineering Department, University of Patras, Rio, Achaia CO 26500 GREECE (e-mail: andrikopg@ece.upatras.gr).

G. Nikolakopoulos is with the Control Engineering Group, Luleå University of Technology, SE-97187 Luleå, Sweden (e-mail: georgios.nikolakopoulos@ltu.se).

S. Manesis is with the Electrical and Computer Engineering Department, University of Patras, Rio, Achaia CO 26500 GREECE (e-mail: stam.manesis@ece.upatras.gr).

978-1-4673-2529-5/12/$31.00 ©2012 IEEE

change during operation and the force that it exerts will be presented. The purpose of this study is to present the insufficiency of the existing PAM modeling approaches and propose novel additional considerations for future model improvements that will best describe the relationship between force, displacement and non-linear thermal properties of PAM actuation, and will result in a significant improvement of the overall model accuracy and in superior and more accurate control schemes.

The article is structured as follows. In Section II, the most significant modifications and improvements on geometric modeling of McKibben PAMs are being presented. In Section III, the main components of the experimental setup are presented, while in Section IV, the overall experimental procedure is described. In Section V, the experimental results that prove the influence of the thermodynamic effects on PAMs elongations are been depicted. In Sections VI and VII the conclusions are drawn and the current work in progress is highlighted, respectively.

II. Geometric Modeling

McKibben, as he has been quoted by other authors in [4], [5], first provided a force equation for the actuator with the double helically wound fiber shell.

In Fig. 2, the basic geometrical characteristics of PAM are presented. L is the tube length, D is the bladder diameter and θ is the braid angle, i.e. the angle between the helical fiber element length and the longitudinal axis of the actuator.

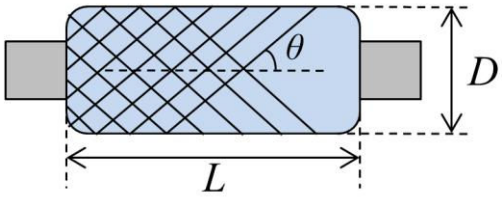

Fig. 2. Simplified geometrical model of PAM.

As shown in (1), tension F is described as linearly proportional to relative pressure P, i.e. the absolute internal gas pressure minus the environment pressure, and a monotonic function of braid angle θ, i.e. the angle between the helical fiber element length and the longitudinal axis of the actuator.

$$F = \frac{\pi D_0^2 P\left[3\cos^2\theta - 1\right]}{4} \tag{1}$$

where D_0 is the diameter when θ=90°.

In the process of deriving the above geometric model the following assumptions are made: a) the actuator is a perfect cylinder with zero-wall-thickness, b) the threads in the sheath are inextensible and always in contact with the outside diameter of the latex bladder, c) latex tubing forces are negligible and d) frictional forces between the tubing and the sheath and between the fibers of the sheath are negligible, thus, assuming that the PAM's temperature remains constant during operation [3].

Schulte, as seen in [4], modified McKibben's original force theoretical relationship for the double helix model and added inner tube elasticity k_e and friction coefficients u_s and u_{st} for friction phenomena between the fibers of the sheath and between the tubing and the sheath, respectively. The resulting force equation is presented below:

$$\begin{aligned} F = {} & \frac{\pi D_0^2 P\left[3\cos^2\theta - 1\right]}{4} \\ & + \pi D_0 k_e \left[L\sin\theta - \frac{\pi\cos^2\theta}{\sin\theta}(D_0\sin\theta - D_r) \right] \\ & - \pi D_0 L(P - P_i)(u_s + u_{st})\sin\theta \end{aligned} \tag{2}$$

where D_r is the resting, i.e. initial, tube diameter; and P_i is the pressure required to achieve an unconstrained tube diameter equal to that of the constrained actuator tube.

Chou and Hannaford, in [3], also modified (1), by considering an effect due to the thickness of the shell and bladder, and eventually producing (3), which added accuracy to the cost of a more complex model.

$$\begin{aligned} F = {} & \frac{\pi D_0^2 P\left[3\cos^2\theta - 1\right]}{4} \\ & + \pi P\left[D_0 t_k \left(2\sin\theta - \frac{1}{\sin\theta} \right) - t_\kappa^2 \right] \end{aligned} \tag{3}$$

where t_k is the shell and bladder thickness.

Caldwell et al., as seen in [11], included the end-cap surface area to account for variation in minimized force generating capability, thus, modifying (1) and resulting to (4).

$$F = \frac{Pb^2\cos^2\theta}{2B^2\pi} - \frac{Pb^2\sin^2\theta}{4B^2\pi} \tag{4a}$$

$$F = \frac{\pi D^2 P(3\cos^2\theta - 1)}{4} \; if\; \theta > \sin^{-1}\frac{D_{cap}}{D} \tag{4b}$$

$$F = \frac{\pi D^2 P(2D^2\cos^2\theta - D_{cap}^2)}{4} \; if\; \theta < \sin^{-1}\frac{D_{cap}}{D} \tag{4c}$$

where b is the helical fiber length, B is the number of trapezoids of the muscle braid, D is the theoretical maximum PAM diameter and D_{cap} is the diameter of the PAM cap.

Tondu and Lopez, in [12], utilized similar geometric description of the PAM with [4] and developed another geometric model (5) with the addition of an empirical factor k to account for the end deformation of PAM.

$$F = \pi\left(\frac{D_r}{2}\right)^2 P\left[a(1-\varepsilon)^2 - b\right] \tag{5}$$

where $a = \frac{3}{\tan^2 \theta_0}, b = \frac{1}{\sin^2 \theta_0}, \varepsilon = \frac{L_0 - L}{L_0}, \varepsilon_{\max} = \frac{1}{k}\left(1 - \sqrt{\frac{b}{a}}\right)$ and L_0, θ_0 are the initial nominal length and the initial braid angle, respectively.

III. Setup Components

For the purposes of the experimental procedures that will be described in the next section, a rotational antagonistic test–bed configuration was constructed as the main part of the experimental setup shown in Fig. 3. This biologically inspired configuration type is widely utilized in the scientific literature for dynamic experimentation and force-position control of PAMs [9], [12], [13]. The presented setup consists of two PAMs on the vertical position with their upper end cap fixed on duralumin plates; and their lower end cap attached to each other via steel wire that is wrapped around a pulley. The PAM on the right side of Fig. 3 is the PAM under study and the one on the left side will play the role of a variable load. The setup also utilizes two proportional pressure regulators with integrated pressure sensors, a laser distance sensor, a load cell, an infrared thermal imaging camera and a data acquisition card.

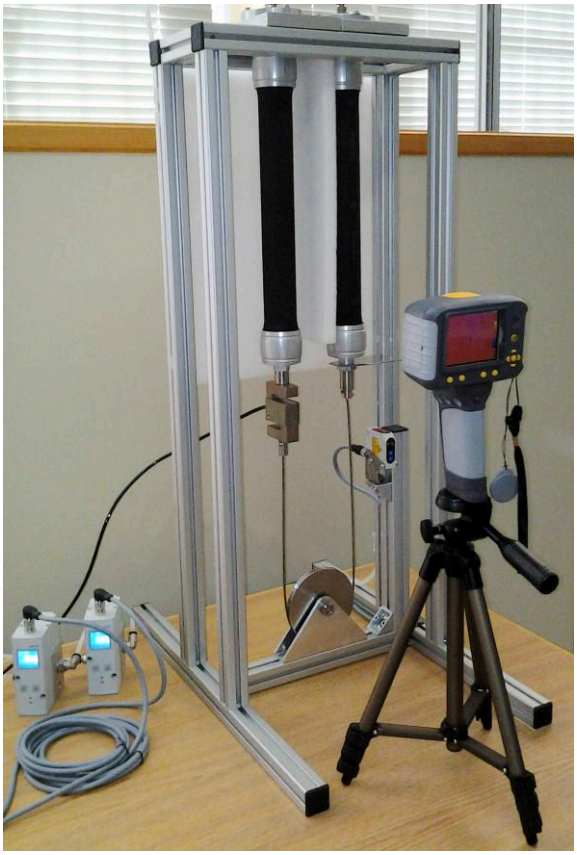

Fig. 3. Layout of the utilized experimental setup.

Specifically, the PAMs utilized in this test–bed are two Festo MXAM-40-AA-DMSP-40-305N-AM-CM fluidic PAMs with 40mm of internal diameter and 305mm of nominal length. Two Festo VPPM-8L-L-1-G14-0L10H-V1P-S1 proportional pressure regulators are used to control and measure the pressure of the compressed air supplied into the PAMs. A Festo SOEL-RTD-Q50-PP-S-7L laser distance sensor is utilized to measure the under study PAM's displacement in the vertical axis. A Zemic H3-C3-300*kg* alloy steel S-type load cell is used to measure the force exerted from the antagonistic operation of the PAMs. Thermal images of the setup are being captured throughout the experiments by an Irisys IR16DS thermal imaging camera. The control of the setup's operation, as well as the data acquisition, is achieved by a National Instruments USB–6215 data acquisition card, while the setup's programming is carried out in National Instruments LabVIEW software.

IV. Experimental Procedure

A. Thermal Imaging

Thermal images of the setup are captured throughout the experiments described in this section, at specific time intervals, in order to analyze PAM surface temperature change during long-run operation and empirically pinpoint the relationship between displacement and force variations with respect to temperature.

Thermal imaging has always been a challenge in experimental environments due to several factors that introduce external disturbances, which consequently increase the marginal error of temperature measurements. For that reason, several steps were taken, prior to the experiments, to ensure minimum disturbance variations and maximum measurement accuracy.

High density macromolecule foam was properly placed around the setup in order to achieve heat insulation of the PAMs from the background environment and from each other during operation.

In order to minimize temperature measurement errors, the thermal camera was calibrated by taking into account the emissivity and reflectivity of the studied materials, thus, correcting the effect of reflected background energy and compensating for additional thermal measurement variations.

Emissivity ε, meaning the ratio of energy radiated by PAM's surface to energy radiated by a black body at the same temperature and with the same surroundings, was set at 0.9 corresponding to the neoprene and aramid synthetic materials that form the outer braided shell of Festo PAMs.

Reflected temperature was set equal to the ambient temperature which was controlled at all times and ranged between 16.5 to 17 degrees Celsius.

All the proposed experiments took place during night hours for minimum environmental thermal disturbances to which infrared cameras are in general considerably sensitive.

B. Zero and Variable Loading Contraction Study

The test PAM, initially at relaxed state with its surface temperature equal to the environment temperature, is subjected to sequential contractions-extensions under sinusoidal pressure input; while the stretching PAM remains

contracted at a constant pressure. In this case, the stretching PAM provides variable loading throughout the test PAM's long-run movement. The experimental procedure followed in this study resembles a pattern of initially auxotonic and finally isometric muscle contractions. The experiment is repeated several times, after restoring the test PAM to its initial temperature state, in order to ensure the uniformity of the results.

Pressure, load and displacement data of the test PAM are recorded while thermal images of the setup are taken at specific time intervals and at the points when the test PAM reaches zero input pressure.

For further analysis of the thermal results collected from the variable loading contraction study, a zero loading contraction study is also conducted where the test PAM's lower end is freely suspended and the PAM is under the same pressure input for the same amount of time.

C. *Constant Test Pressure - Forced Stretching Study*

In this experiment, the test PAM, initially at relaxed state with its surface temperature equal to the environment temperature, remains contracted under a constant test pressure and is subjected to sequential forced stretches by the antagonistic PAM, which contracts under pulse pressure inputs that steadily increase in amplitude, playing in every stage the role of a static load. The experiment continues until the test PAM reaches its nominal length and is repeated after specific time intervals, during which the test PAM is subjected to sequential variable loading contractions-extensions, causing its surface temperature to rise.

The test PAM is then subjected to sequential contractions-extensions under the same input characteristics of the variable loading contraction study. After a specific operation time, the static loading study is repeated and the whole experimental process starts again in the same way and for several repetitions.

Pressure, load and displacement data of the test PAM are being recorded while thermal images of the setup are captured before every static loading experiment with the test PAM in relaxed state.

The purpose of this experiment is to construct the force-displacement relationship for a specific test pressure and for different surface temperatures. By repeating this experiment after constant and a priori defined time windows, the effects of the temperature on the PAM's extraction length could be easily being observed as it will be presented in the next Section.

V. Experimental Results

A. *Zero and Variable Loading Contraction Study*

The first phase of the experiments had the test PAM subjected to sequential contractions-extensions under sinusoidal pressure input of 0 to 5bar outlier range, 4sec period and 50% duty cycle; and with zero loading since its lower end was freely suspended. Thermal pictures of the setup were captured throughout the experiment while the change of temperature on the PAM's surface can be observed in the following sequential images depicted in Fig. 4 with respect to the experimentation time.

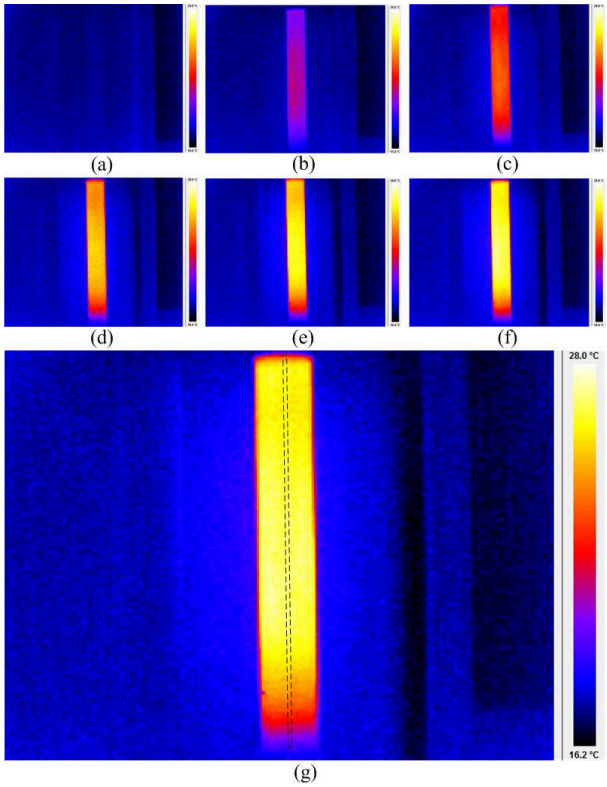

Fig. 4. PAM surface temperature change during zero loading contraction study and after (a) idle condition, (b) 1 minutes, (c) 2 minutes, (d) 4 minutes, (e) 6 minutes, (f) 8 minutes and (g) 16 minutes of operation. The dashed black rectangular in (g) depicts the thermal data extraction area.

For the extraction of the thermal data, the curve temperature effect was taken under consideration, where generally curved surfaces and, in this case, cylindrical ones, appear in thermal images to have lower temperature in their optical edges. For that reason, and by assuming that the PAM's surface temperature is uniformly distributed along circular cross-sections of the tube, temperature analysis was focused on a vertical line of thermal pixels that aligns with PAM's longitudinal axis from the camera's optical viewpoint; as seen in Fig. 4(g).

Fig. 5 shows the extracted thermal data and, specifically, the surface temperature change along the longitudinal axis of the test PAM with respect to (operation time). The pneumatic connection on the upper end cap of the muscle corresponds to zero length and the lower end cap, which is freely suspended, corresponds to the nominal length of 305mm. Mainly due to frictional forces because of the aramid and neoprene weaving intense and complex relative motion, the temperature begins to steadily increase. Parallel heat dissipation from the braided shell to the environment and to the inner pressurized air that rapidly enters and exits the PAM tube isn't enough to result in gradual cool down.

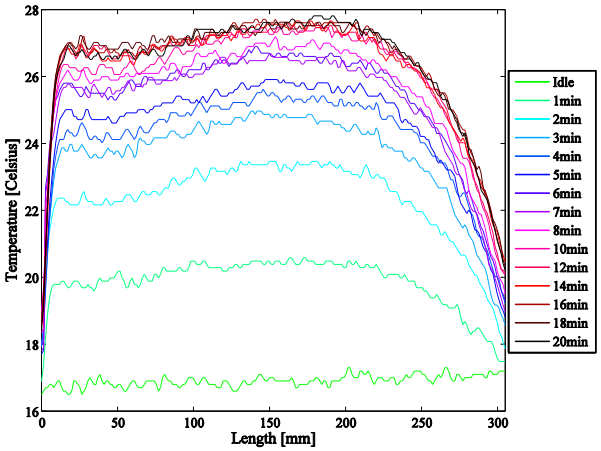

Fig. 5. Lengthwise temperature change of the test PAM's surface during zero loading contraction study with respect to minutes of operation time.

Progressively, a non-uniform increase in temperature is observed and that uneven thermal distribution becomes even more intense as the operation time increases. The temperature appears to be greater when near the pneumatic connection, than towards the freely suspended end, where a larger slope decrease is observed. Furthermore, a more acute increase in temperature is concentrated around the middle section of the muscle, reaching the local maximum value at approximately two thirds of PAM length.

Elastomeric materials such as neoprene present viscoelastic properties and a first explanation to the uneven temperature distribution phenomenon can be given if the neoprene polymer is observed at a molecular level. The atoms in the Methylene (CH_2) groups of neoprene threads that are closer to the middle section of the PAM tube perform more symmetric stretching vibrations while those closer to the end caps perform more bending vibrations [14]. The absorption frequency in the infrared plane is larger in stretching vibrations as it requires more energy to stretch (or compress) a bond than to bend it [15]. Thus, the infrared frequency absorption becomes larger in scale in the middle section, causing the temperature to rise more than that of the sections closer to the end caps.

An additional consideration of the larger thermal energy dissipated by the air flow entering through the pneumatic connection, would explain the increased temperature of the section closer to the pneumatic connection in comparison to the temperature of the section closer to the other end cap.

Under these experimental conditions, the PAM seems to reach a point of thermal saturation at around 16 minutes of operation as the temperature reaches its maximum values along the entire length. The total maximum increase in temperature was recorded at approximately 11° Celsius.

The second phase of the experiments had the test PAM subjected to sequential contractions-extensions under the same input characteristics; while the stretching PAM remains contracted at a constant pressure of 3bar, playing the role of a variable load.

The surface temperature change along the longitudinal axis of the test PAM with respect to minutes of operation time is shown in Fig. 6. The pneumatic connection on the upper end cap of the muscle corresponds to zero length and the lower end cap, which is now under variable loading, corresponds to the nominal length of 305mm. Similar uneven thermal distribution is observed but to a greater scale, since the test PAM is under variable load ranging from zero to around 1400N; and its movement becomes highly strenuous resulting in more intense frictional forces between the threads of the braided shell and between the threads and PAM inner bladder.

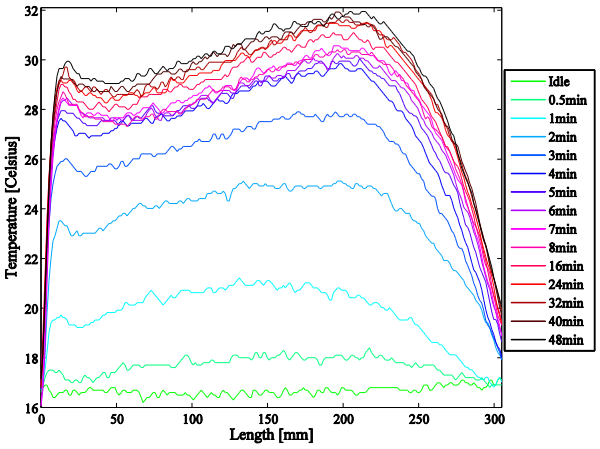

Fig. 6. Lengthwise temperature change of the test PAM's surface during variable loading contraction study with respect to minutes of operation time.

Further comparison between the thermal data of the zero and variable loading contraction studies, presented in three-dimensions in Fig. 7, shows that in the second case the temperature increase escalates faster and even further; thermal distribution appears even larger in the middle section of the PAM and reaches maximum temperature at about two thirds of its length. Under these experimental conditions, the

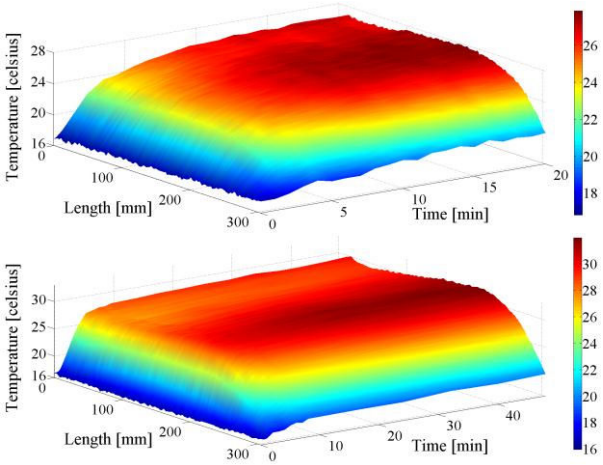

Fig. 7. Three-dimensional representation of the PAM's surface temperature change zero loading (upper diagram) and variable loading (lower diagram) contraction studies with respect to length of the elastic tube and minutes of operation time.

PAM seems to reach a point of thermal saturation at around 50 minutes of operation as the temperature reaches its maximum values along the entire length. The total maximum increase in temperature was recorded at approximately 15° Celsius.

PAM's non-linear characteristics as (a) the bladder materials' viscoelasticity, (b) friction between the weaving and the bladder and between the threads of the double helix weaving and (c) the conical deformation of the tubes edges, result to force/displacement hysteresis phenomena. Throughout the variable loading contraction study, test PAM's displacement and force data were been recorded and extracted in order to pinpoint if, how much and in what way does the force/displacement hysteresis loop alters with respect to operation time and, subsequently, temperature change. Those experimentally verified alterations are depicted in the hysteresis loops presented in Fig. 8.

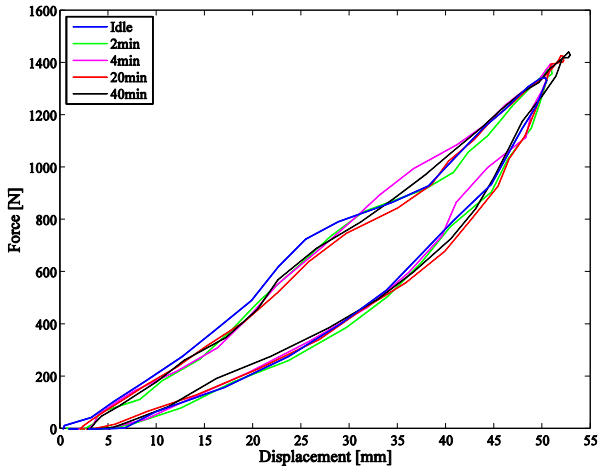

Fig. 8. Force-Displacement hysteresis loop change with respect to minutes of operation time.

Specifically, a shift of the hysteresis loop to greater values of force and displacement, with respect to operation time, is observed. The difference between the maximum force and displacement values of the idle condition and those of the test PAM's condition after 40minutes of work was approximately 98N and 2.3mm, respectively. An interesting observation is that another shift happens also at zero loading, where the displacement appears to be non-zero, despite zero test pressure during that state. These hysteresis alterations are assumed to be originated from the bladder materials' viscoelastic properties alteration with respect to temperature.

Due to thermal motion, the secondary bonds of the polymer material used in PAMs constantly break and reform. The deformed polymer's viscoelastic properties change with respect to temperature. Under constant stress, an increase in temperature causes a logarithmic decrease in the time required to impact equal strain. That stress-strain relationship, also known as the creep modulus, decreases with increasing temperature as it takes less work to stretch a viscoelastic material an equal distance than it takes at a lower temperature [16]. These viscoelastic phenomena, under the same pressure input characteristics, result in increased conical deformation and bladder stretching, thus, increasing the maximum displacement and, subsequently, the force exerted from the PAM.

B. Constant Test Pressure - Forced Stretching Study

In the final phase of the experiments, the goal is to construct the force-displacement relationship for a specific test pressure and for different surface temperatures.

In Fig. 9 the force-displacement relationship for a test pressure of 2 bar is presented. The experiment is repeated after every 16 minutes of operation (under the same input characteristics of the variable loading contraction study). The repetition of the experiment after specific operation time shows a measurable increase in the force-displacement relationship, where, after 48 minutes of operation, the maximum force appears increased by approximately 150N and the displacement by approximately 3mm.

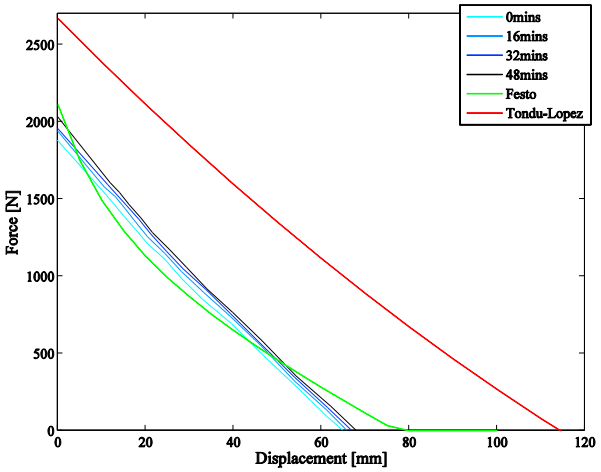

Fig. 9. Force-Displacement relationship change with respect to minutes of operation time and with comparison to Festo Co. and Tondu-Lopez force models.

In the same figure and for comparison reasons, plotted beside the experimental data is the relationship provided from Festo Co. for the specific muscle model that was used in the experiments and the Tondu-Lopez force-displacement model that was described in (5). Both of these models don't take temperature change into account. Specifically, Festo's model appears to have more intense curvature and the difference between that model and experimental data increases towards zero force and maximum displacement. That difference further increases in the case of Tondu-Lopez geometric model, a result that justifies the growing need for PAM model improvements that would take into account the changing characteristics in the force-displacement relationship due to non-linear phenomena like temperature increase with relation to operation time, viscoelastic material properties and frictional forces.

VI. Work in Progress

Mathematical confirmation and incorporation of the presented experimental results to an improved force-

displacement equation that will take viscoelastic properties and temperature dependence into account is work in progress. Further experimentation with PAMs of different nominal diameters and lengths as well as extensive variable and static loading studies is also part of current work.

VII. Conclusions

The acquired experimental results showed that the viscoelastic material properties and friction phenomena from the braid mesh threads relative motion and their contact with the inner elastic bladder cannot be assumed negligible, as they can be held responsible for non-linear increase of temperature with respect to operation time and uneven thermal distribution along the longitudinal axis of the PAM. These phenomena further result to quite significant change in material viscoelastic properties, which, subsequently, cause changes in the PAM force-displacement relationship. The obtained results fulfilled the purpose of this study, which was to propose additional considerations for future PAM model improvements that would best describe the relationship between force, displacement and non-linear thermodynamic properties of PAM actuators.

References

[1] R. Pierce, “Expansible cover,” U.S. Patent No. 2211478,1940.

[2] P. Warszawska. “Artificial pneumatic muscle.” Dutch patent No. 6704918, 1967.

[3] C. P. Chou and B. Hannaford, “Measurement and modeling of McKibben pneumatic artificial muscles,” IEEE Transactions on Robotics and Automation, vol. 12, no. 1, pp. 90-102, 1996.

[4] H. F. Schulte, “The characteristics of the McKibben artificial muscle,” The Application of External Power in Prosthetics and Orthotics, pp. 94-115, 1961.

[5] R. H. Gaylord, “Fluid Actuated Motor System and Stroking Device.” US Patent no. 2,844,126, 22 July 1958.

[6] J. Yarlott, “Fluid actuator,” US Patent No. 3 645 173, 1972.

[7] V. Nickel, J. Perry, and A. Garrett, “Development of useful function in the severely paralyzed hand,” Journal of Bone and Joint Surgery, vol. 45-A, no. 5, pp. 933–952, 1963.

[8] B. Hannaford and J. M. Winters, “Actuator properties and movement control: biological and technological models,” in Multiple Muscle Systems: Biomechanics and Movement Organization, New York, 1990, pp. 101–120.

[9] G. Andrikopoulos, G. Nikolakopoulos, and S. Manesis, “A Survey on Applications of Pneumatic Artificial Muscles”, in 19th Mediterranean Conference on Control and Automation, June 20-23, Corfu, Greece, 2011.

[10] E. Kelasidi, G. Andrikopoulos, G. Nikolakopoulos, and S. Manesis, “A Survey on Pneumatic Muscle Actuators Modeling”, in 20th IEEE International Symposium on Industrial Electronics (ISIE 2011), Gdansk, Poland, 2011.

[11] D.G. Caldwell, N. Tsagarakis and G.A. Medrano-Cerda, “Bio-mimetic actuators: polymeric pseudo muscular actuators and pneumatic muscle actuators for biological emulation,” Mechatronics 10, 499-530, 2000.

[12] B. Tondu and P. Lopez “Modeling and control of McKibben artificial muscle robot actuators.” IEEE Control Systems Magazine, 20(2):15–38, 2000.

[13] S. Davis, “Braid Effects on Contractile Range and Friction Modeling in Pneumatic Muscle Actuators,” The International Journal of Robotics Research, vol. 25, no. 4, pp. 359-369, Apr. 2006.

[14] T. Shimanouchi, "Local and overall vibrations of polymer chains", Pure Applied Chemistry, Vol. 36, No. 1-2 (1973)

[15] D. Steele, "Theory of vibrational spectroscopy", W.B. Saunders, 1971.

[16] N. G. McCrum, C. P. Buckley and C. B. Bucknall, “Principles of Polymer Engineering”, Oxford University Press, Second Edition, 1997.